ChemComm

Accepted Manuscript

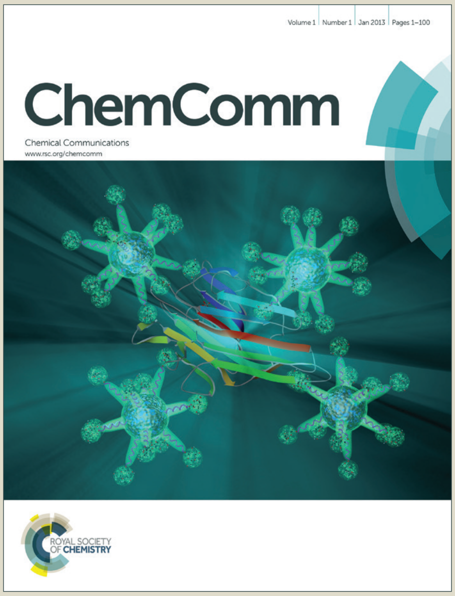

ROYAL SOCIETY OF **CHEMISTRY**

www.rsc.org/chemcomm

Journal Name RSCPublishing

COMMUNICATION

Cite this: DOI: 10.1039/x0xx00000x

MFI zeolite nanosponges possessing uniform mesopores generated by bulk crystal seeding in the hierarchical surfactant-directed synthesis

Received 00th January 2012,
Accepted 00th January 2012

DOI: 10.1039/x0xx00000x

www.rsc.org/

Changbum Jo,[a] Kanghee Cho,[a] Jaeheon Kim,[a,b] and Ryong Ryoo*[a,b]

The synthesis of mesoporous material with uniform mesopore diameters and crystalline MFI zeolite walls has been achieved, simply by seeding the multiammonium surfactant-directed synthesis with bulk zeolite crystals. The bulk seeds disappeared in the final product. As a result of seeding, the mesoporous zeolite could be generated rapidly even at high Al content.

Synthetic zeolites are widely used as catalysts in petrochemical industry. Recently, ultrathin MFI zeolite nanosheets were synthesized using multi-ammonium surfactant molecules as the structure-directing agent (SDA) that could function in meso and micro length scales simultaneously.[1,2] This discovery brought about a renewed interest in zeolites as a new class of mesoporous materials. The thickness of the zeolite nanosheets could be tailored by changing the number of ammonium groups in the SDA, and thicknesses as small as 1.5 nm were obtained.[3] These nanosheets exhibited superior performance to bulk zeolite in various applications such as in heterogeneous catalysts and filtration membranes, where rapid diffusion through zeolite micropores was important.[4,5] In addition to the efficient use of micropores, the zeolite nanosheets possessed strong Brønsted acid sites at the external surfaces.[6] The external acid sites were accessible through open mesopores between neighbouring nanosheets. This suggests new possible applications for these materials as catalysts for reactions involving bulky molecules.[7]

The MFI nanosheets are obtained so far as disordered assemblies or regular stacks of multiple layers supported by surfactant layers.[1] The former are called “unilamellar MFI nanosheets,” and the latter “multilamellar.” The unilamellar zeolite can be calcined safely at high temperatures to remove the organic structure-directing agent while maintaining the mesoporosity between adjacent nanosheets. However, the pore size distribution (PSD) was very broad, in the range from 4 to 30 nm.[1] In the multilamellar zeolite, the distance between neighbouring nanosheets was very uniform, but this was until before calcination. Upon calcination, the zeolite layers condensed so that the mesopore between nanosheets was almost completely lost. The collapse of the layered mesostructure could be prevented by supporting the interlayer region with silica pillars.[2] The pillared MFI nanosheets possessed mesopores of very uniform diameters. The mesopore diameters can be tailored by adjusting the tail length of the SDA surfactant. However, such post-synthetic pillaring is a time-consuming strategy that requires complicated processing steps. Additionally, these silica pillars were unstable in water. The pillars were disintegrated by the humidity in the atmosphere when stored for several months under ambient conditions. The nanosheets layers also collapsed easily when the sample was compressed. Recently, Tsapatsis *et al.* reported the synthesis of self-pillared pentasil zeolite using tetrabutylphosphonium hydroxide as the zeolite SDA.[8] This zeolite was made of orthogonally connected MFI/MEL nanosheets. Nevertheless, this zeolite had a broad distribution of mesopores (2–15 nm). Moreover, the Al content in this zeolite was difficult to increase beyond an Si/Al ratio of 75.

Another problem with the surfactant-directed MFI nanosheets is the long hydrothermal reaction times required for synthesis. This is of particular concern in materials with high Al content. Crystallization times longer than two weeks were required for MFI nanosheets with Si/Al < 20, during which the multiammonium surfactant could decompose by Hoffman elimination under the strongly basic synthesis conditions. Usually, SDA decomposition resulted in the formation of bulk MFI zeolite. Therefore, in the present work, we attempted to decrease the hydrothermal synthesis time by adding a small amount of bulk MFI zeolite into the synthesis reaction gel as a crystallization-accelerating seed.[9-11] The result was five-time rapid generation of MFI nanosheets. Even at Si/Al = 15, the synthesis took less than 6 d at 150 °C. Additionally, the bulk zeolite particle additives disappeared completely from the nanosheet product. More importantly, the MFI product was obtained with a nanosponge-like morphology with mesopores of uniform diameter. The mode value of the mesopore diameters could be controlled by the alkyl tails in the structure-directing surfactant (typically 2.5–4.3 nm for C_{12} – C_{22}). These MFI zeolite nanosponges exhibited excellent hydrothermal and mechanical stabilities.

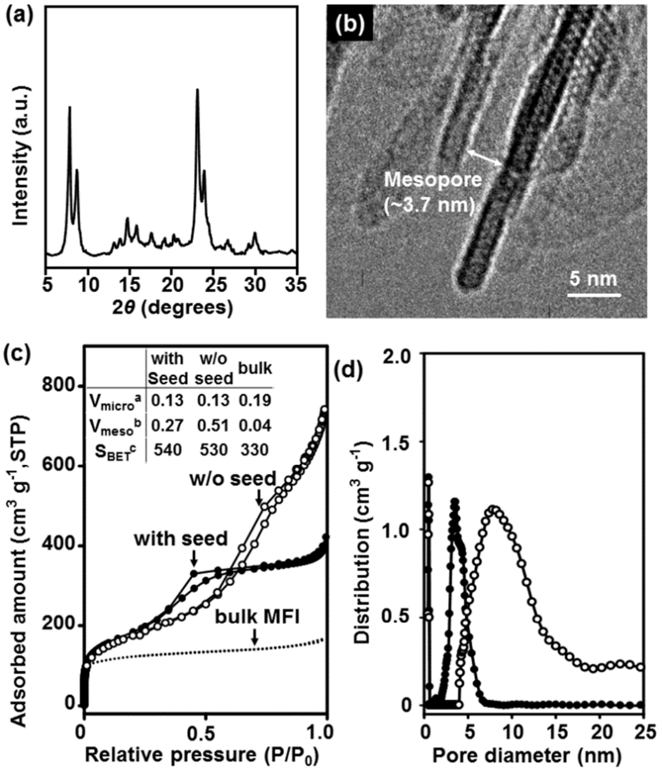

Figure 1. Structure characterization data for a representative calcined-ZNS sample (*i.e.* with seed) with Si/Al = 20 synthesized using the $C_{18\text{-}6\text{-}6}$ SDA and bulk MFI seeds at 150 °C for 2.5 d, including (a) XRD pattern, (b) TEM image, (c) Ar adsorption-desorption isotherm, and (d) pore size distribution. In (c) and (d), the ZNS sample (black circle) is compared with the control sample (white circle) synthesized without seeding, and bulk MFI zeolite (dotted line). $^{a}V_{micro}$ and $^{b}V_{meso}$ are the micropore volume (cm^3/g) and mesopore volume (cm^3/g) evaluated from the NLDFT, respectively. $^{c}S_{BET}$ is the BET surface area (m^2/g) obtained from Ar adsorption.

In a typical synthesis batch of the zeolite nanosponges (denoted by ZNSs), a commercial ZSM-5 zeolite sample with Si/Al ratio of 15 (Zeolyst, CBV 3024E) was used as the seed. This ZSM-5 zeolite is composed of aggregates of 100–200 nm bulk crystals. 0.1 g of this calcined zeolite (amounting to 5 wt.% of the total silica source) was dispersed in 17.0 mL of a 1.1 M aqueous solution of NaOH in a polypropylene bottle. The mixture was stirred for about 10 h at 60 °C, and then, 1.6 g of $[C_{18}H_{37}–N^{+}–(CH_3)_2–C_6H_{12}–N^{+}(CH_3)_2–C_6H_{13}]Br_2$ ($C_{18\text{-}6\text{-}6}$ for short; synthesis of this component is detailed in the Supporting Information) was dissolved. In an another polypropylene bottle, 17.1 g of distilled water, 0.49 g of $Al_2(SO_4)_3•18H_2O$ (Aldrich), and 0.7 mL of 47% sulphuric acid were mixed until a clear solution was obtained. Then, the contents of the two bottles were combined in a single pour, and the resulting mixture was magnetically stirred for 1 h. This solution was added with 6.3 g of tetraethoxysilane (Junsei) at once. The mixture was vigorously shaken by hand, and subsequently aged overnight at 60 °C. The resultant gel had the following molar composition: 100 SiO_2/ 2.5 Al_2O_3/ 7.5 $C_{18\text{-}6\text{-}6}$/ 18 H_2SO_4/ 30 Na_2O/ 4000 H_2O. This mixture was heated for an adequate time (typically, 2.5 d) at 150 °C, in a tumbled autoclave, until the formation of zeolite. For comparison purposes, an unseeded control sample was synthesized in the same manner; the hydrothermal reaction took 11 d. Small aliquots of the reaction mixture were collected after various intervals during hydrothermal reaction. Each sample was analysed using powder X-ray diffractometry (XRD), scanning electron microscopy (SEM), high-resolution transmission electron microscopy (HRTEM), ^{27}Al solid-state NMR, and Ar adsorption-desorption isotherm. The adsorption isotherm was analysed using nonlinear density functional theory (NLDFT) to obtain the cumulative pore volume plot and the PSD.

MFI zeolites without any amorphous residue were obtained after 11 d of hydrothermal reaction at 150 °C when crystal seeding was not employed. When the synthesis was seeded with 5 wt.% bulk MFI zeolite, the required time for crystallization decreased to 2.5 d. The Si/Al ratios of both the seeded and unseeded samples were the same (19 ± 1). Both zeolite samples were composed of 2.5-nm thick MFI zeolite nanosheets, as determined by the XRD data and the SEM, TEM images (Figure 1, Figures S1 and S2 in SI). However, there were significant differences in the pore textural properties (Figures 1c and 1d). The control sample exhibited a broad distribution of mesopore diameters (5 – 25 nm). The total pore volume was 0.6 cm^3 g^{-1}. This pore texture is characteristic of an MFI sample with unilamellar nanosheet morphology. In the case of seeded zeolite sample (*i.e.*, ZNS), a very narrow peak centred at 3.5 nm was shown in PSD result. Furthermore, the mode value of the mesopore diameters could be tailored over the range of 2.5 - 4.3 nm using C_{12} – C_{22} alkyl groups, as is the case with pillared MFI zeolites (Figure S3 in SI). This result indicated that the individual nanosheets were arranged in such a nanosponge-like morphology, in which the adjacent nanosheets were supported by each other even after the removal of surfactant by calcination. In good agreement with the nanosponge mesostructure, a low-angle XRD peak was present at 2*θ* = 1.2° as a shoulder on the background (Figure S4 in SI) for the calcined ZNS samples. This peak was very broad compared to that of the pillared MFI nanosheets because the ZNS was composed of narrow, short nanosheets, as shown in the TEM images.

Our synthesis result raised the question of why zeolite nanosponges with uniform mesopore diameters could be generated using the seeding process. To find a clue to this question, we compared the XRD patterns and PSDs of the solid precipitates collected during the ZNS synthesis according to the hydrothermal reaction time (*i.e.*, o d, 2.5 d, or 11 d). This investigation revealed that the initial gel (reaction time = o d) had an ordered hexagonal mesostructure with amorphous walls, similar to MCM-41 (Figure S5 in SI). The MCM-41-like mesophase transformed into the ZNS phase exhibiting a small-angle XRD shoulder after 2.5 d, as mentioned before. This ZNS sample exhibited a very narrow PSD peak, which was very similar to the PSD in the initial MCM-41-like sample. Upon further treatment lasting 11 d, the basic structure of the solid precipitate was still MFI nanosheet, but the nanosheets became conspicuously wider than in the ZNS materials. The nanosheets formed a random assembly with a wide distribution of intersheet mesopores over 3–15 nm (*i.e.*, unilamellar MFI nanosheets). As this result shows, the materials underwent consecutive transformations from MCM-41 to ZNS and unilamellar MFI. A notable difference from our earlier work on unseeded zeolites is that noncrystalline lamellar mesophase was not detected between the MCM-41 aluminosilicate and MFI nanosheet. This difference should be relevant to the rapid zeolite formation and the similarity of mesopore diameters between MCM-41 and ZNS. Based on these observations, it is reasonable to think that the bulk zeolite seeds could disintegrate into numerous subnanometre nuclei. These nuclei could be embedded everywhere in the MCM-41 pore walls and could thereby start zeolite formation. This is comparable to the pseudomorphic crystallization of zeolite. We believe that the nanosheets size could increase with time through zeolite dissolution and recrystallization, similar to the Ostwald ripening process.[12]

Figure 2 shows two magic-angle-spinning ^{27}Al NMR spectra taken from a ZNS sample with Si/Al = 15. The ZNS sample was prepared using the aforementioned synthesis procedure, except for a change in the Si/Al ratio (to 15) and the reaction time (to 6 d). The NMR spectra were collected after moistening the samples with distilled water as-synthesized and after calcination, respectively. The spectrum from the as-synthesized sample exhibited an intense signal at 54 ppm (Figure 2a). This peak was assigned to the AlO_4 unit with tetrahedral coordination in the zeolite framework.[13] There appeared to be no distinct signal at 0 ppm that would be assigned to extra-framework Al with octahedral coordination. This result indicates that almost all Al atoms were located inside the zeolite framework. After calcination, the NMR spectrum showed a low-intensity peak at 0 ppm and a shoulder-like signal around 30 ppm (Figure 2b). The latter can be assigned to a penta-coordinated Al species.[14] The appearance of the penta-coordinated and octahedral Al signals can be attributed to dealumination from the zeolite framework during the calcination process. Nevertheless, as judged by the result in Figure 2, the extent of dealumination was insignificant in the ZNS.

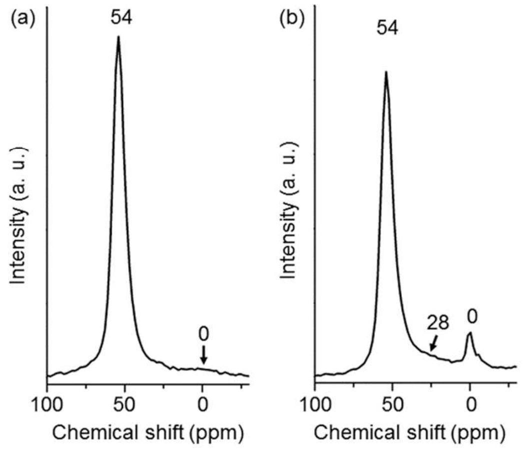

Figure 2. ^{27}Al solid-state NMR spectra of (a) as-synthesized and (b) calcined ZNS samples with an Si/Al ratio of 15.

The mechanical stability of the ZNS was tested and compared with that of the previously reported pillared MFI nanosheets. In this stability test, each calcined sample was compressed for 10 min at a fixed pressure using a stainless-steel die. The mesopore volume of the sample was determined by Barrett-Joyner-Halenda adsorption cumulative pores between 1.7 nm and 30 nm in diameter using N_2 adsorption isotherms. The mechanical stability was assessed as the loss of the mesopore volume as a result of compression. The test was repeated at various intervals while increasing the compression pressure from 125 to 625 MPa. The results showed that ZNS was much more stable than pillared MFI nanosheets, against compression (Figure S6 in SI). The pillared MFI lost its mesopore volume more than 50% at 250 MPa, but the ZNS sample compressed at 250 MPa exhibited only a 30% loss of mesopore volume. More than 50% of the original mesopore volume was retained, even after compression at 625 MPa. In addition to its high mechanical stability, the ZNS sample exhibited great hydrothermal stability compared to the pillared MFI. The porosity of the ZNS sample did not change conspicuously after treating the samples in boiling water (100 °C) for 5 d, but the pillared MFI sample lost its mesoporosity completely within 1 d under these conditions.

Conclusions

The bulk zeolite particle additives must have disintegrated into sub-nanometre nuclei, which acted as seeds for the rapid formation of MFI zeolite nanosponge in surfactant-directed synthesis. The mesopores of the zeolite nanosponge are not as highly ordered as in mesoporous MCM-41 materials, but the nanosponge has a very narrow distribution of mesopores, comparable to that of MCM-41. The mesopore walls can be tailored to a uniform thickness by the surfactant SDAs, which can be inferred from the result of previous works using the surfactant-directed synthesis. In addition, the mesopore walls can have an ion-exchange capacity and strong acidity of the zeolite framework. The ZNS samples exhibited a significantly high catalytic activity for decalin cracking. This result indicates the presence of strong acid sites on the framework of the mesopore walls (see Figure S7 in SI). These characteristics are highly desirable for applications in catalysis and adsorption. Furthermore, we believe that the present strategy of seeding with bulk crystals should be extended to the synthesis of other nanomorphic zeolites, whether or not the nanoscale morphology is generated by a SDA-type surfactant or an organosilane surfactant. Though we have not reported it here, high-quality mesoporous MOR, FAU and CHA zeolites can be synthesized using organosilane surfactants by the aid of bulk zeolite seeding. We expect that surfactant-directed nanomorphic zeolites with various structures could be available as a family of uniformly mesoporous materials in the near future.

Notes and references

[a] Center for Nanomaterials and Chemical Reactions, Institute for Basic Science (IBS), Daejeon 305-701, Korea.

[b] Department of Chemistry, KAIST, Daejeon 305-701, Korea

†This work was supported by Institute for Basic Science (IBS) [CA1301].

Electronic Supplementary Information (ESI) available: Synthesis procedures for multiammonium surfactants, Characterization results for MFI nanosheets in non-seeded system, XRD and PSD results of precipitates depending on reaction time. See DOI: 10.1039/c000000x/

1. M. Choi, K. Na, J. Kim, Y. Sakamoto, O. Terasaki, R. Ryoo, *Nature* 2009, **461**, 246.
2. K. Na, M. Choi, W. Park, Y. Sakamoto, O. Terasaki, O. R. Ryoo, R. *J. Am. Chem. Soc.* 2010, **132**, 4169.
3. J. Jung, C. Jo, K. Cho, R. Ryoo, *J. Mater. Chem.* 2012, **22**, 4637-4640.
4. J. Kim, W. Kim, Y. Seo, J. C. Kim, R. Ryoo, *J. Catal.* **2013**, 301, 187.
5. K. Varoon, X, Zhang, B. Elyassi, D. D. Brewer, M. Gettel, S. Kumar, J. A. Lee, S. Maheshwari, A. Mittal, C. Y. Sung, M. Cococcioni, L. F. Francis, A. V. McCormick, K. A. Mkhoyan, M. Tsapatsis, *Science*, 2011, **334**, 72.
6. Y. Seo, K. Cho, Y. Jung, R. Ryoo, *ACS catal.* 2013, **3**, 713.
7. W. Kim, J. C. Kim, J. Kim, Y. Seo, R. Ryoo, *ACS. Catal*. 2013, **3**, 192.
8. X. Zhang, D. Liu, S. Asahina, K. A. Cychosz, K. V. Agrawal1, Y. A. Wahedi, A. Bhan1, S. A. Hashimi, O. Terasaki, M. Thommes, M. Tsapatsis, *Science*, 2012, **336**, 1684.
9. B. Xie, J. Song, L. Ren, Y. Ji, J. Li, F. -S. Xiao, *Chem. Mater.* 2008, **20**, 4533.
10. R. D. Edelman, D. V. Kudalkar, T. Ong, J. Warzywoda, R. W. Thompson, *Zeolites* 1989, **9**, 496.
11. Y. Kamimura, S. Tanahashi, K. Itabashi, A. Sugawara, T. Wakihara, A. Shimojima, T. Okubo, *J. Phys. Chem. C* 2011, **115**, 744.

12. K. Na, W. Park, Y. Seo, R. Ryoo, *Chem. Mater.* 2011, **23**, 1273.
13. C. A. Fyfe, G. C. Gobbi, J. S. Hartman, J. Klinowski, J. M. Thomas, *J. Phys. Chem.*, 1982, **96**, 1247.
14. G. Majano, L. Delmotte, V. Valtchev, S. Mintova, *Chem. Mater.*, 2009, **21** (18), 4184.